JACS
JOURNAL OF THE AMERICAN CHEMICAL SOCIETY
pubs.acs.org/JACS
Article

Structure-Guided Designing Pre-Organization in Bivalent Aptamers

Xiaoli Hu,[⊥] Linlin Tang,[⊥] Mengxi Zheng,[⊥] Jian Liu, Zhe Zhang, Zhe Li, Quan Yang, Shoubo Xiang, Liang Fang, Qiao Ren, Xuemei Liu, Cheng Zhi Huang,* Chengde Mao,* and Hua Zuo*

Cite This: J. Am. Chem. Soc. 2022, 144, 4507−4514

Read Online

ACCESS | Metrics & More | Article Recommendations | Supporting Information

ABSTRACT: Multivalent interaction is often used in molecular design and leads to engineered multivalent ligands with increased binding avidities toward target molecules. The resulting binding avidity relies critically on the rigid scaffold that joins multiple ligands as the scaffold controls the relative spatial positions and orientations toward target molecules. Currently, no general design rules exist to construct a simple and rigid DNA scaffold for properly joining multiple ligands. Herein, we report a crystal structure-guided strategy for the rational design of a rigid bivalent aptamer with precise control over spatial separation and orientation. Such a pre-organization allows the two aptamer moieties simultaneously to bind to the target protein at their native conformations. The bivalent aptamer binding has been extensively characterized, and an enhanced binding has been clearly observed. This strategy, we believe, could potentially be generally applicable to design multivalent aptamers.

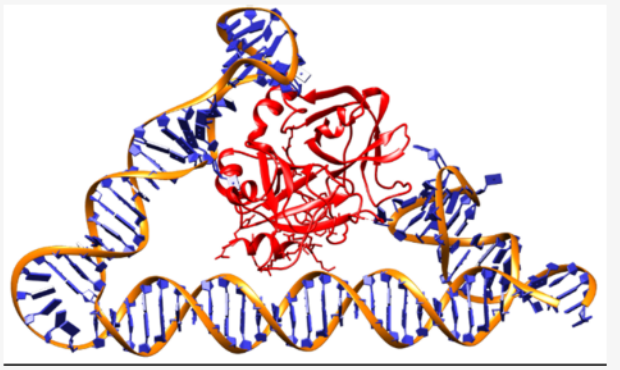

INTRODUCTION

Aptamers can specifically recognize cognate ligands and provide alternatives to antibodies for molecular recognition.[1,2] Compared with antibodies, aptamers have many desirable advantages. They are chemically synthesized, rendering their productions to be inexpensive, batch-to-batch consistent, and in large quantity. Aptamers are also chemically and structurally stable. They can be stored for long time and do not lose their activities because of thermal denaturation. Because of these advantages, aptamers promise a great range of applications including biosensing, disease diagnosis and treatment, and drug delivery.[3−9] However, aptamers generally have substantially lower binding affinities than antibodies have.[10,11] This intrinsic problem for aptamers is due to the limited chemical scope of nucleic acids (only four unique components: A, G, T/U, and C). In contrast, antibodies have 20 different types of residues. Improving the aptamer affinity is critically needed for realizing their full potentials.

One straightforward approach to increase the binding avidity is *via* multivalency.[12,13] This strategy is commonly observed in biological systems, such as cell−cell interactions.[13−15] It is also exploited in engineering systems.[16−19] For example, a trivalent D-Ala−D-Ala/vancomycin interaction could reach a K_d value of 10^{-15} M, while an individual D-Ala−D-Ala/vancomycin interaction only has a weak binding (K_d: ~10^{-5} M).[17] The key to the great success is pre-organization.[20] (i) Multiple interactions are linked in such a way that each individual interaction can be satisfied without spatial/orientational stress, thus no enthalpy loss. (ii) The multivalent binding partners have no dramatic conformational change during binding, thus only minimal entropy loss. In previous studies, people applied the multivalency concept to improve the binding affinity of aptamers, for example, the thrombin aptamer.[21−31] However, those designs can be further improved. When the linkers are too flexible (such as single-stranded DNA linkers), the two aptamer moieties in the bivalent aptamer can randomly move (translationally and rotationally) relative to each other. Upon binding to the ligand, those motions are lost, leading to a significant loss in entropy. In other cases, the orientations/separations of the two aptamers are not optimized to simultaneously bind to the ligand. There is a significant stress in the complex, leading to a significant loss in enthalpy. In either case, the benefit of multivalency is not fully realized.

Herein, we report a rational design of a pre-organized, bivalent thrombin aptamer (bApt) based on the crystal structures of two orthogonal aptamer−thrombin (T) complexes and structural DNA nanotechnology. Two different types of DNA aptamers, HD22[32,33] and RE31,[34−36] bind to two distinct sites of thrombin and do not interfere with each other. The crystal structures of both aptamer−thrombin complexes was available.[33,36] Based on the crystal structures, we hypothesize that if using a rigid DNA

Received: November 30, 2021
Published: March 4, 2022

https://doi.org/10.1021/jacs.1c12593
J. Am. Chem. Soc. 2022, 144, 4507−4514

linker to link the two aptamers together while maintaining the location and orientation of the two aptamers relative to thrombin, we would get a high-avidity, bivalent aptamer.

RESULTS AND DISCUSSION

Figure 1 shows the design process (Scheme S1):

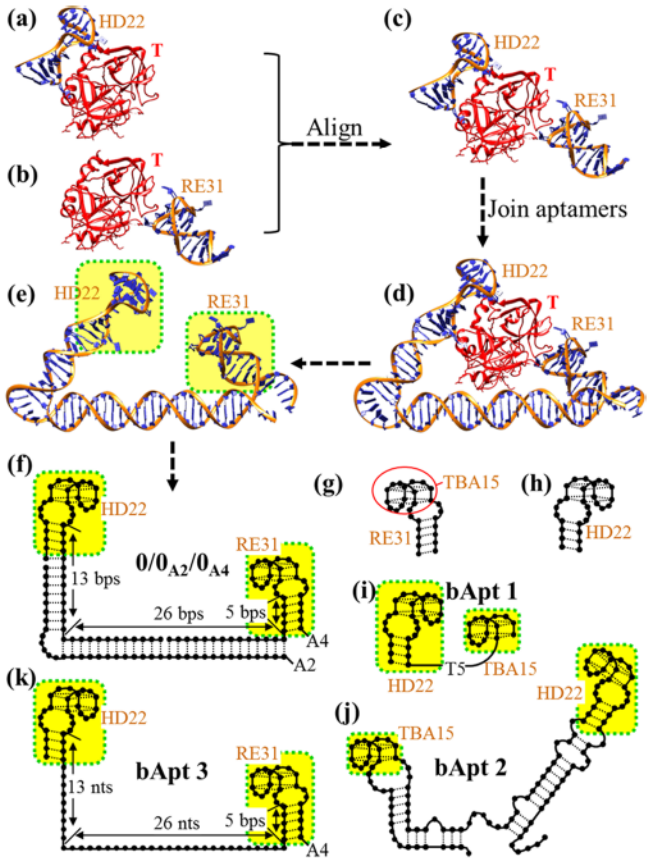

Figure 1. Design of a pre-organized, bApt: $0/0_{A2}/0_{A4}$. Crystal structures of a thrombin (T) complex with (a) HD22 and (b) RE31. The thrombin is shown in the same orientation in (a) and (b). (c) Aligning the two crystal structures according to thrombin. (d) Designing a semi-rigid, DNA linker to join the two aptamers. The model (e) and secondary structure (f) of the designed bivalent aptamer, $0/0_{A2}/0_{A4}$. Secondary structures of aptamers (g) RE31, (h) HD22, two previously reported bivalent aptamers (i) bApt 1 and (j) bApt 2, and (k) another control bivalent aptamer bApt 3 with an ssDNA linker. The red circle in (g) is aptamer TBA15.

(1) We start with the crystal structures of two individual aptamer−thrombin (T) complexes, HD22-T complex (PDB ID: 4i7y, Figure 1a) and RE31-T complex (PDB ID: 5cmx, Figure 1b).[33,36] RE31 is a variation of the commonly known thrombin aptamer TBA15.[37] In addition to the TBA15 portion, RE31 has a short duplex stem that facilitates the design of the bivalent aptamer (Figure 1g).[34]

(2) In Coot,[38] a computer software of biomacromolecule modeling, the two crystal structures are aligned together by superimposing thrombin (Figure 1c).

(3) In the aligned structure, the two aptamers are separated from each other by thrombin. It is impossible to directly connect the two aptamers by a simple, rigid DNA duplex because of the steric hindrance of thrombin. To make the connection, ideal B-form DNA duplex models are generated by Coot and then aligned to HD22 to elongate the duplex region of HD22. Another ideal B-form DNA duplex of adequate length is visually translated and rotated in Pymol to dock for potential strand connections. Excess regions of the two duplex models are trimmed and the strands are reconnected. The final design of the bivalent aptamer is bridged from HD22 to RE31 by three DNA duplex domains of 13, 26, and 5 base pairs (bps) (Figure 1d,e and S1−S3).

(4) The DNA linker has two sharp turns, which is achieved by two additional elements. (i) At the lower left corner, a 5-nucleotide (nt)-long, single-stranded DNA (ssDNA) loop is introduced. Such a loop can bend DNA duplexes by roughly 60−90°.[39,40] (ii) At the lower right corner, one strand is broken and two single-stranded, oligo-adenine tails (A2 or A4) are introduced to the DNA ends. Those ssDNA tails prevent the two flanking duplexes from stacking onto each other and allow the DNA duplexes to bend here.

The designed bivalent aptamer is dubbed as $0/0_{A2}/0_{A4}$. The three numbers indicate the length differences (bps) of the three helical domains (left, central, and right) from the designed lengths shown in Figure 1f. All bApt control molecules (will be discussed later) are named according to such differences. Subscripted A*n* following the second and the third numbers indicate the oligo-adenine tails on the central and right helical domains, respectively. $0/0_{A2}/0_{A4}$ still has a certain desirable degree of flexibility, which may correct some minor modeling errors and position the aptamers to the optimal positions/orientations. Overall, in the designed bivalent aptamer, the two individual aptamer moieties (HD22 and RE31) are linked by a semi-rigid DNA bridge, and each aptamer binds to thrombin at its native conformation. A rigid complementarity between the bivalent aptamer and thrombin in terms of both shape and binding site is expected. Because of the pre-organization of the aptamer moieties, the overall conformation of the bivalent aptamer would not significantly change upon binding to thrombin. Thus, a high binding avidity would be expected.

We thoroughly examined the designed bivalent aptamer, $0/0_{A2}/0_{A4}$, using native polyacrylamide gel electrophoresis (nPAGE), atomic force microscopy (AFM), isothermal titration calorimetry (ITC), and light scattering spectra (Figure 2). In the characterization, five control aptamers (Figure 1g−k) were used for comparison. HD22 and TBA15 are two extensively studied, monovalent aptamers. Two bivalent aptamers (bApt 1 and bApt 2) are reported in the literature. In bApt 1, a flexible T5 linker was used to match the distance between the two binding sites on thrombin.[30] bApt 2 was evolved in an in vitro selection.[31] bApt 3 mimics $0/0_{A2}/0_{A4}$ except for containing a flexible, ssDNA linker instead of a semi-rigid, duplex DNA linker. We first analyzed the aptamer−thrombin binding by nPAGE (Figure 2a). A short hairpin was used as a loading control, which corresponded to the bands at the bottom of the gel. All aptamers appeared as sharp bands with migration mobilities expected as their respective molecular weights. When incubated with thrombin under our experimental condition, however, the aptamers behaved very differently. All aptamers associated with thrombin to form aptamer−T complexes. Both monovalent aptamers (HD22 or TBA15) show a fuzzy band corresponding to Apt−T complexes with low intensities, indicating that the monovalent Apt−T

https://doi.org/10.1021/jacs.1c12593
J. Am. Chem. Soc. 2022, 144, 4507−4514

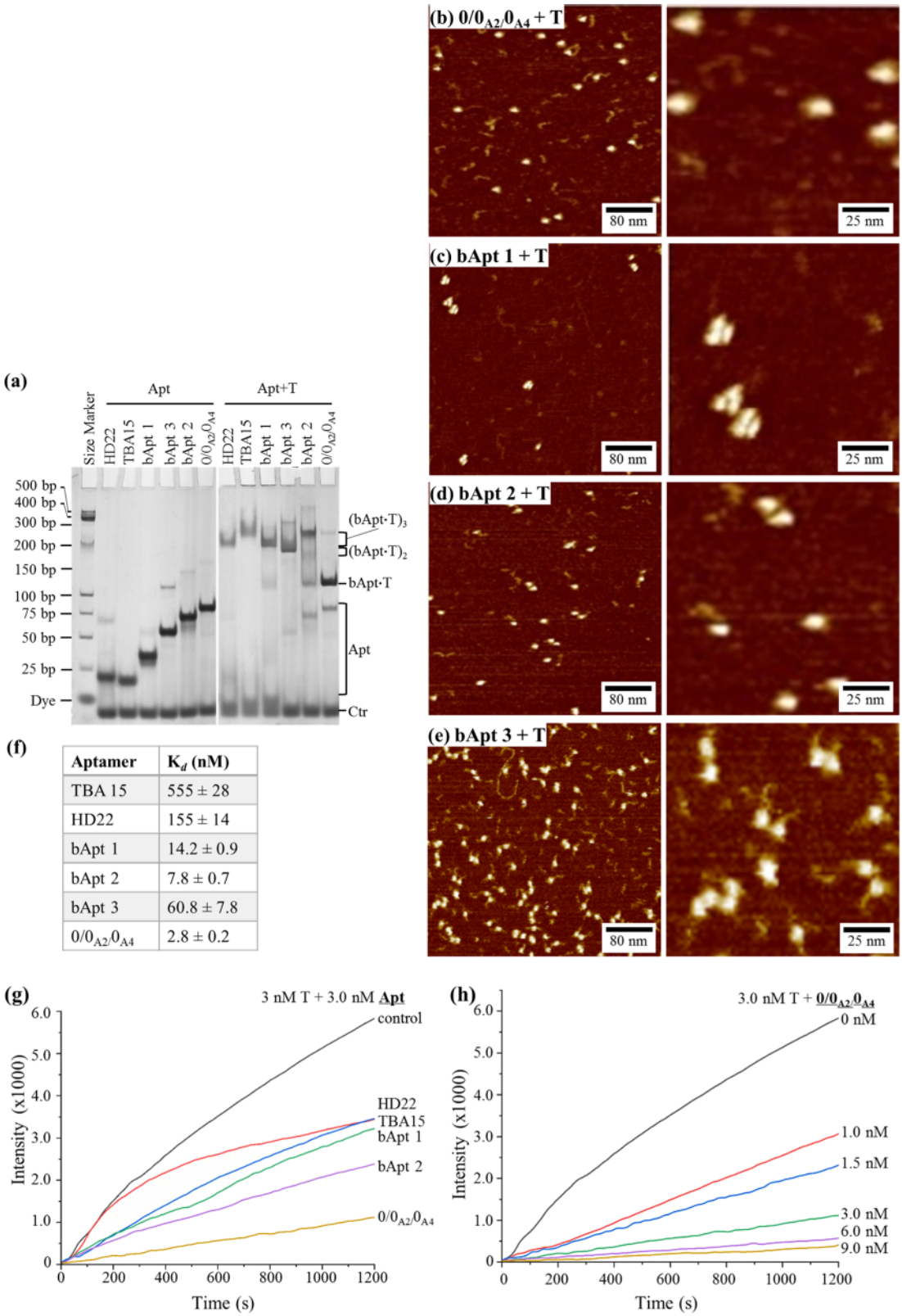

Figure 2. Characterization of the designed bivalent aptamer $0/0_{A2}/0_{A4}$. (a) Native polyacrylamide gel (6%) electrophoretic analysis of the binding between DNA aptamers (Apt) and thrombin (T). (b–e) Atomic force microscopy visualization of bApt–T complexes (samples incubated at a molar ratio of 1:1). Each is shown with a pair of AFM images at two different magnifications. (f) Dissociation constants (K_d) of the Apt–T complexes were determined by isothermal titration calorimetry. Each measurement has been repeated three times. Real-time light scattering spectra of a fibrinogen solution treated with 3 nM thrombin (g) plus 3 nM different aptamers, or (h) plus different concentrations of $0/0_{A2}/0_{A4}$.

complexes were not stable and dissociated during electrophoresis as continuous smears. In contrast, all the four bApts show strong complex bands, suggesting that the bApt–T complexes are stable.

https://doi.org/10.1021/jacs.1c12593
J. Am. Chem. Soc. 2022, 144, 4507–4514

One surprising observation is that the four bApt−T complexes exhibited very different electrophoretic patterns (Figure 2a). The $0/0_{A2}/0_{A4}$−T complex had a sharp, strong band with moderately slower mobility than $0/0_{A2}/0_{A4}$ itself, indicating the formation of a stable 1:1 complex, $0/0_{A2}/0_{A4}$−T. In contrast, the three control bApt−T complexes show fuzzy, multiple bands with much slower mobilities in comparison with either bApts themselves or the $0/0_{A2}/0_{A4}$−T complex, suggesting those that control bApt−T complexes are not conformationally stable and contain multiple copies of bApts and thrombin. Such a compositional difference was further confirmed by AFM imaging (Figures 2b−e and S4−S7). The $0/0_{A2}/0_{A4}$−T complex contained only one single protein (the bright, tall object), consistent with the nPAGE data: the $0/0_{A2}/0_{A4}$−T complex is a 1:1 complex. The three control bApt−T complexes all contain multiple proteins. The complexes bApt 1−T, bApt 2−T, and bApt 3−T contained three, two, and two proteins, respectively. Thus, the three control bApt−T complexes were 3:3, 2:2, and 2:2 complexes for bApt 1, bApt 2, and bApt 3, respectively. (Note that the Apt−T complexes were partially dissociated during the AFM sample preparation.)

The unexpected results for the three control bApts are presumably due to the improper lengths and conformations of the linkers (Figure S8). (i) For bApt 1, the linker is a 5-nt-long ssDNA that can be stretched to 3.35 nm (assuming 0.67 nm/nt).[41] When two aptamers (TBA15 and HD22) bind to a thrombin, the shortest, straight-line distance between the DNA strand ends of the two aptamers is 6.1 nm (Figure S8a). Clearly, the ssDNA linker is too short in bApt 1 to allow the two aptamer moieties of bApt 1 to simultaneously reach and bind to the same thrombin protein. To satisfy both aptamer moieties to bind to thrombin, an alternative, 3:3 complex, $(\text{bApt 1}-\text{T})_3$ (instead of a 1:1 complex) forms in that each bApt 1 can bind to two copies of the protein, and each protein can bind to two copies of bApt 1. (ii) For bApt 3, the linker is a 35-nt-long ssDNA, which is, in principle, long enough when stretched to reach the separation. However, flexible ssDNA chains tend to contract to form random coils due to entropic force. To stretch the ssDNA costs extra energy. A 2:2 complex, $(\text{bApt 3}-\text{T})_2$, avoids such an extra energy, thus becoming the preferred structure. (iii) For bApt 2, the conformation of the semi-rigid linker (mostly DNA duplex), likely, does not properly orient the two aptamer moieties to simultaneously bind to the same protein; instead, they bound to different proteins to form a 2:2 $[(\text{bApt 2}-\text{T})_2]$ or 3:3 complex $[(\text{bApt 2}-\text{T})_3]$.

We have further used ITC to quantitatively measure the binding affinity of these aptamers. Indeed, the rationally designed $0/0_{A2}/0_{A4}$ exhibits excellent binding capability (Figures 2f, S9 and Table S1). Its apparent affinity (K_d: 2.8 nM) is higher than the control bApts (K_d: 14.2, 7.8 nM, 60.8 nM for bApt 1, bApt 2, and bApt 3, respectively) and far higher than monovalent aptamers (K_d: 555 and 155 nM for TBA15 and HD22, respectively) under our experimental conditions.

Furthermore, the designed bivalent aptamer has an enhanced capability to inhibit thrombin as shown by an enzyme assay (Figure 2g,h). Thrombin is a protease and can convert fibrinogen into fibrin to form fibers, leading to strong light scattering intensity. By real-time monitoring the light scattering spectra, thrombin activity can be measured. While all aptamers inhibit thrombin, the bivalent aptamers are more efficient than monovalent aptamers. Particularly, the designed $0/0_{A2}/0_{A4}$ substantially outperforms the controls, bApt 1 and bApt 2 (Figure 2g). The inhibition degree is proportional to the aptamer concentration (Figure 2h). When bApt $0/0_{A2}/0_{A4}$ is in excess (by two times) to thrombin, the thrombin activity decreased by 93%.

All the above characterizations prove that $0/0_{A2}/0_{A4}$ efficiently binds to thrombin and inhibits its enzymatic activity. The key to designing this efficient bivalent aptamer is proper pre-organization. For $0/0_{A2}/0_{A4}$, there are several important structural elements. Any small variation to them would dramatically change the behavior of the bivalent aptamer.

Single-Stranded, Oligo-Adenine Tails (An) at the Lower Right Corner (Figures 3 and S10). In the designed bApt, the two aptamer moieties are connected via a duplex with two sharp turns. The left sharp turn is realized by a 5-nucleotide (nt) long single-stranded loop, and the right turn is realized by single-stranded A*n* tails. To demonstrate the importance of the A*n* tails, we have prepared three control bApts: 0/0/0 with no A*n* tail, $0/0_{A2}/0$ with one A_2 tail, and $0/0_{A2}/0_{A2}$ with two A_2 tails. (i) When there is no A*n* tail (in 0/0/0), the two helical domains will stack onto each other at the nick position to form a pseudo-continuous, straight helix (Figure 3b). In this undesired bApt conformation, the two aptamer moieties are separated far away from each other and thus, cannot bind to the same thrombin protein to form a 1:1 complex bApt−T instead to form a 2:2 complex $(\text{bApt}-\text{T})_2$. (ii) When there are two A*n* tails (in $0/0_{A2}/0_{A2}$ and $0/0_{A2}/0_{A4}$), the two A*n* tails electrostatically repel each other and prevent the two helical domains flanking the nick position from stacking onto each other. Thus, the two helical domains can easily rotate relative to each other and allow the helix to bend at this position (Figure 3b). Consequently, the two aptamer moieties can bind to the same thrombin protein to form a 1:1 complex bApt−T. (iii) When there is only one A*n* tail ($0/0_{A2}/0$), a mixture of a 1:1 complex bApt−T and 2:2 complex $(\text{bApt}-\text{T})_2$ forms. Coarse grain simulation by OxDNA,[42,43] a DNA simulation software, reveals the local conformations of the lower right corners of the bApts (Figure 3b). The formation of the different complexes is confirmed by both nPAGE (Figure 3c) and AFM visualization (Figure 3d−f).

Lengths of the Three Helical Domains. In the designed bivalent aptamer $0/0_{A2}/0_{A4}$, the two aptamer moieties are not only spatially separated to match the separation of the two binding sites of thrombin but also properly oriented to face the binding sites of the thrombin. A change in the length of any helical domain would simultaneously change both the spatial separation between the two aptamer moieties and the aptamer orientations due to the helical nature of the DNA duplexes. They would introduce stresses to prevent the two aptamer moieties from simultaneously binding to the same thrombin, resulting in either lower binding efficiencies or an incapability to form a 1:1 complex bApt−T.

To examine the impact of the left helical domain, we have prepared three control bApt molecules. Compared with $0/0_{A2}/0_{A4}$, the only change in the control molecules is that the left helical domain lengths are either shortened by 2 bps, $(-2/0_{A2}/0_{A4})$ or elongated by 2 bps $(2/0_{A2}/0_{A4})$ or 4 bps $(4/0_{A2}/0_{A4})$. Both nPAGE and AFM imaging show that this subtle variation dramatically changes the bApt−thrombin interaction (Figures 4 and S11). $-2/0_{A2}/0_{A4}$ forms a 1:1 complex bApt−T with thrombin but at a slightly lower binding efficiency than $0/0_{A2}/0_{A4}$. Both $2/0_{A2}/0_{A4}$ and $4/0_{A2}/0_{A4}$ bind to thrombin and form a mixture of 1:1 (bApt−T) and 2:2 $[(\text{bApt}-\text{T})_2]$ complexes.

Similarly, we have demonstrated the impact of the lengths of the middle and right helical domains (Figures 5, S12 and S13) by using two sets of control bApt molecules. One set $(0/-2_{A2}/0_{A4}$,

https://doi.org/10.1021/jacs.1c12593
J. Am. Chem. Soc. 2022, 144, 4507−4514

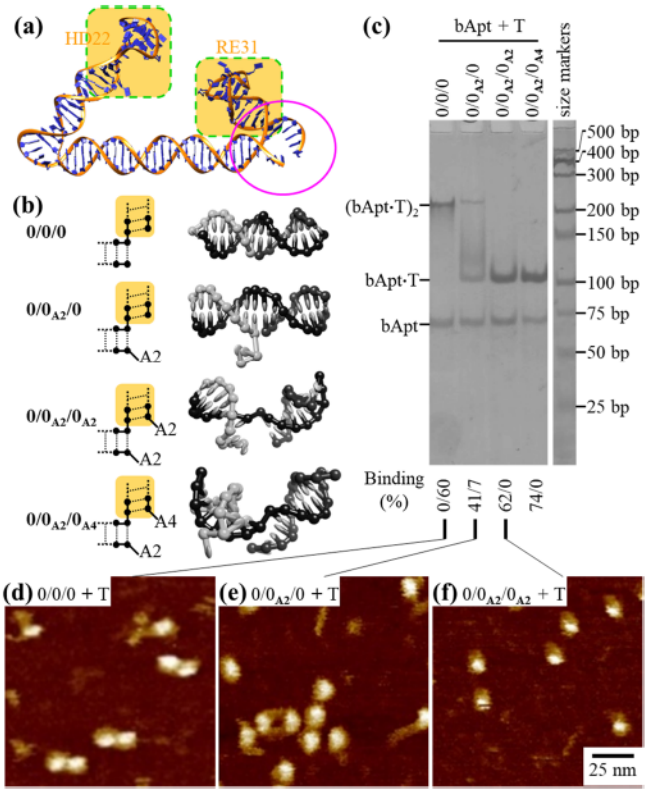

Figure 3. Impact of the single-stranded, oligo-adenine tails at the lower right corner on bApt binding to thrombin. (a) bApt structure with the lower right corner circled. (b) Structural variations of the right lower corner, circled in (a), and their simulated 3D conformations. (c) nPAGE (6%) analysis of binding of bApts and thrombin. The percentages of 1:1 (first number) and 2:2 (second number) complexes formed were calculated from band intensities and listed below the gel image. (d–f) AFM visualization of bApt–thrombin complexes (samples incubated at ratio 1:1).

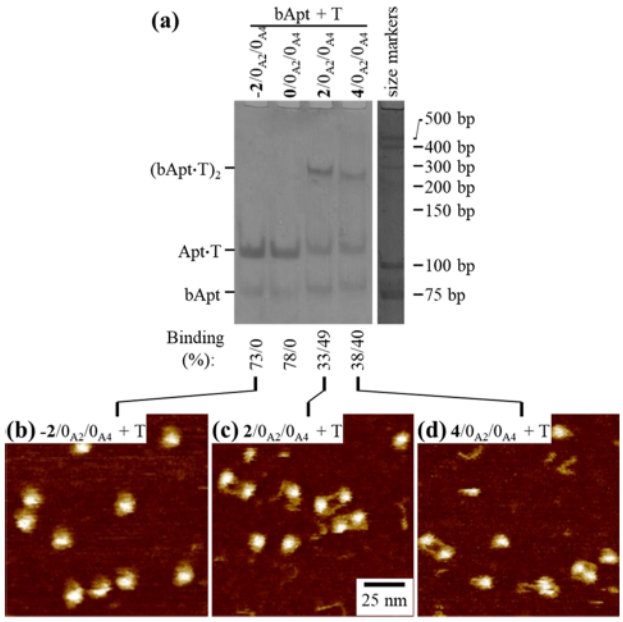

Figure 4. Impact of the length of the left helical domain on bApt binding to thrombin. (a) nPAGE (6%) analysis. (b–d) AFM visualization of bApt–T complexes.

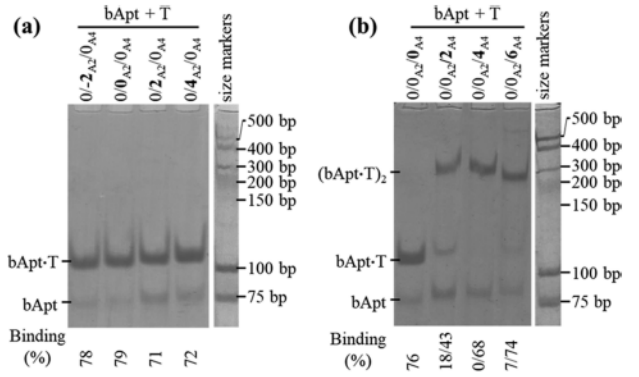

Figure 5. nPAGE (6%) analysis of the impact on the lengths of the middle (a) and right (b) helical domains on bApt binding to thrombin.

$0/2_{A2}/0_{A4}$, and $0/4_{A2}/0_{A4}$) is for studying the middle helical domain, and the other ($0/0_{A2}/2_{A4}$, $0/0_{A2}/4_{A4}$, and $0/0_{A2}/6_{A4}$) is for the right helical domain. While the middle helix only has a minor influence (Figures 5a and S12), the right helix influences quite substantially (Figures 5b and S13). When elongating the right helical domain by 2 bps, the resulting bApt–T complex will change from 1:1 (bApt–T) to 2:2 [$(bApt–T)_2$].

This strategy is potentially a generally applicable strategy as long as one molecule has multiple binding events and the corresponding structural information is available. To demonstrate this point, we apply this strategy to another system (Figure 6). An RNA aptamer, Corn, can bind to thioflavin T (ThT) and greatly enhance the fluorescence of ThT. A crystallography study reveals that Corn RNA forms homodimers and ThT binds to the interface of the Corn dimer.[45] One ThT molecule simultaneously contacts two copies of the Corn RNA aptamer. Based on this structural information, we hypothesize that we can

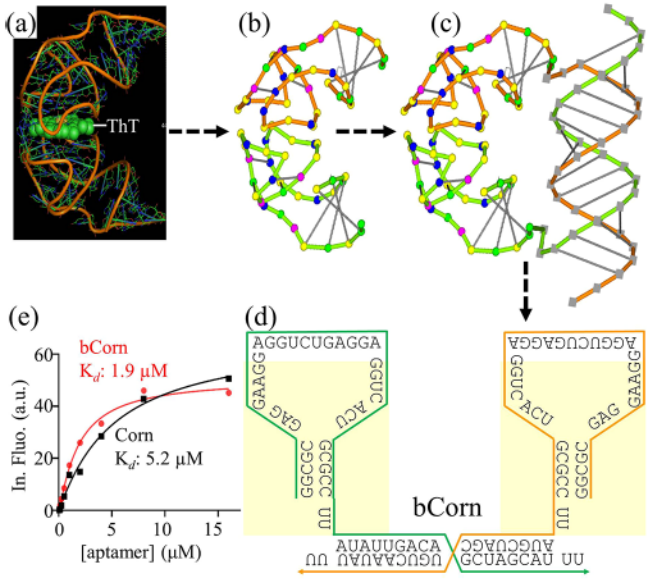

Figure 6. Bivalent Corn RNA aptamer. (a) Crystal structure of the Corn RNA aptamer–Thioflavin (ThT) complex. (b) Simplified representation of the Corn RNA homodimer prepared by Tiamat.[44] (c) An RNA duplex domain is designed to covalently join the two copies of original Corn RNAs into a stable bivalent Corn RNA aptamer (bCorn). (d) Secondary structure of the designed bCorn. Each shaded rectangle represents an original Corn moiety. (e) Binding curves of original Corn (black) and bCorn (red) against ThT.

https://doi.org/10.1021/jacs.1c12593
J. Am. Chem. Soc. 2022, 144, 4507–4514

engineer a stable bivalent Corn RNA aptamer (bCorn) by linking the original Corn aptamers to a stable RNA duplex of a proper length. In the designed bCorn, the two Corn moieties are positioned in such a way as to bind to ThT at the position and orientation mimicking those in the crystal. A higher binding affinity is expected for bCorn than for original Corn. The dissociation constant (K_d) values were experimentally determined to be 1.9 and 5.2 μM for bCorn and the original Corn, respectively (Figure 6e), confirming that bCorn has a higher affinity than original Corn does.

CONCLUSIONS

Herein, we have developed a structure-guided strategy to rationally design bApts with pre-organized interactions. It simultaneously maximizes the enthalpy gain and minimizes the entropic loss. The resulting bApt can efficiently bind to thrombin and inhibit its enzymatic activity. This study demonstrates that multivalency is not just simply linking multiple interactions together. Instead, these interactions need to be properly organized in both spatial separation and relative orientation to achieve complementarity between two multivalent binding partners.[30,33] Such aspects are often not implemented. We believe that this could potentially become a general strategy for improving aptamer binding affinity. Many proteins have multiple aptamers and some proteins form homo-oligomers. They all provide chances for the current strategy. One current limitation is that the structural information of the individual binding event is required. Though it is not always available now, rapid methodology development in structural characterization (e.g., CryoEM imaging) and structure prediction (e.g., AlphaFold from DeepMind) would quickly acquire such information.

ASSOCIATED CONTENT

Supporting Information

The Supporting Information is available free of charge at https://pubs.acs.org/doi/10.1021/jacs.1c12593.

Materials and methods and additional experimental data (PDF)

AUTHOR INFORMATION

Corresponding Authors

Cheng Zhi Huang − *Key Laboratory of Luminescence Analysis and Molecular Sensing (Southwest University), Ministry of Education, College of Pharmaceutical Sciences, Southwest University, Chongqing 400715, China;* orcid.org/0000-0002-1260-5934; Email: chengzhi@swu.edu.cn

Chengde Mao − *Key Laboratory of Luminescence Analysis and Molecular Sensing (Southwest University), Ministry of Education, College of Pharmaceutical Sciences, Southwest University, Chongqing 400715, China; Department of Chemistry, Purdue University, West Lafayette, Indiana 47907, United States;* orcid.org/0000-0001-7516-8666; Email: mao@purdue.edu

Hua Zuo − *Key Laboratory of Luminescence Analysis and Molecular Sensing (Southwest University), Ministry of Education, College of Pharmaceutical Sciences, Southwest University, Chongqing 400715, China;* orcid.org/0000-0002-8461-8988; Email: zuohua@swu.edu.cn

Authors

Xiaoli Hu − *Key Laboratory of Luminescence Analysis and Molecular Sensing (Southwest University), Ministry of Education, College of Pharmaceutical Sciences, Southwest University, Chongqing 400715, China;* orcid.org/0000-0003-4006-786X

Linlin Tang − *Key Laboratory of Luminescence Analysis and Molecular Sensing (Southwest University), Ministry of Education, College of Pharmaceutical Sciences, Southwest University, Chongqing 400715, China;* orcid.org/0000-0002-6337-4363

Mengxi Zheng − *Department of Chemistry, Purdue University, West Lafayette, Indiana 47907, United States;* orcid.org/0000-0002-1625-6663

Jian Liu − *Key Laboratory of Luminescence Analysis and Molecular Sensing (Southwest University), Ministry of Education, College of Pharmaceutical Sciences, Southwest University, Chongqing 400715, China;* orcid.org/0000-0002-5071-8307

Zhe Zhang − *Key Laboratory of Luminescence Analysis and Molecular Sensing (Southwest University), Ministry of Education, College of Pharmaceutical Sciences, Southwest University, Chongqing 400715, China;* orcid.org/0000-0001-7465-163X

Zhe Li − *Department of Chemistry, Purdue University, West Lafayette, Indiana 47907, United States;* orcid.org/0000-0001-9402-4940

Quan Yang − *Department of Cardiology, The Fourth People's Hospital of Sichuan Province, Chengdu 610016, China;* orcid.org/0000-0002-9740-9704

Shoubo Xiang − *Key Laboratory of Luminescence Analysis and Molecular Sensing (Southwest University), Ministry of Education, College of Pharmaceutical Sciences, Southwest University, Chongqing 400715, China;* orcid.org/0000-0001-8364-0764

Liang Fang − *Department of Oncology, The Ninth People's Hospital of Chongqing, Chongqing 400700, China;* orcid.org/0000-0002-6230-0100

Qiao Ren − *Key Laboratory of Luminescence Analysis and Molecular Sensing (Southwest University), Ministry of Education, College of Pharmaceutical Sciences, Southwest University, Chongqing 400715, China;* orcid.org/0000-0002-1933-0160

Xuemei Liu − *Key Laboratory of Luminescence Analysis and Molecular Sensing (Southwest University), Ministry of Education, College of Pharmaceutical Sciences, Southwest University, Chongqing 400715, China;* orcid.org/0000-0002-4638-2716

Complete contact information is available at: https://pubs.acs.org/10.1021/jacs.1c12593

Author Contributions

⊥X. H., L.T. and M.Z. contributed equally to this work.

Notes

The authors declare no competing financial interest.

ACKNOWLEDGMENTS

This article is dedicated to the memory of Prof. Nadrian (Ned) Seeman, the founder of Structural DNA Nanotechnology, for his inspiration, mentorship, and friendship. This work was financially supported by the NSFC (22134005 and 21974111), the NSF (2025187 and 2107393), and the

Chongqing Research Program of Basic Research and Frontier Technology (cstc2020jcyjmsxmX0947, cstc2021jcyj-msxmX1033, and -msxmX0931). C.Z.H. was supported by the Chongqing Talents Program for Outstanding Scientists (No.cstc2021ycjh-bgzxm 0178) and H.Z. was supported by the Venture & Innovation Support Program for Chongqing Overseas Returnees (cx2018088). We would like to thank Prof. Jianxiang Zhang for assistance with Isothermal Titration Calorimetry analysis and Prof. Xun Gou for the use of ITC (MicroCal iTC200, GE Healthcare) in College of Life Science, Sichuan Normal University, China.

REFERENCES

(1) Hermann, T.; Patel, D. J. Adaptive Recognition by Nucleic Acid Aptamers. *Science* **2000**, *287*, 820−825.
(2) Zhou, J.; Rossi, J. Aptamers as targeted therapeutics: current potential and challenges. *Nat. Rev. Drug Discov.* **2017**, *16*, 181−202.
(3) Li, S.; Jiang, Q.; Liu, S.; Zhang, Y.; Tian, Y.; Song, C.; Wang, J.; Zou, Y.; Anderson, G. J.; Han, J.-Y.; Chang, Y.; Liu, Y.; Zhang, C.; Chen, L.; Zhou, G.; Nie, G.; Yan, H.; Ding, B.; Zhao, Y. A DNA nanorobot functions as a cancer therapeutic in response to a molecular trigger in vivo. *Nat. Biotechnol.* **2018**, *36*, 258−264.
(4) Zhu, G.; Zheng, J.; Song, E.; Donovan, M.; Zhang, K.; Liu, C.; Tan, W. Self-assembled, aptamer-tethered DNA nanotrains for targeted transport of molecular drugs in cancer theranostics. *Proc. Natl. Acad. Sci. U.S.A.* **2013**, *110*, 7998−8003.
(5) Savla, R.; Taratula, O.; Garbuzenko, O.; Minko, T. Tumor targeted quantum dot-mucin 1 aptamer-doxorubicin conjugate for imaging and treatment of cancer. *J. Control. Release* **2011**, *153*, 16−22.
(6) Thevendran, R.; Sarah, S.; Tang, T.-H.; Citartan, M. Strategies to bioengineer aptamer-driven nanovehicles as exceptional molecular tools for targeted therapeutics: A review. *J. Control. Release* **2020**, *323*, 530−548.
(7) Sprengel, A.; Lill, P.; Stegemann, P.; Bravo-Rodriguez, K.; Schöneweiß, E.-C.; Merdanovic, M.; Gudnason, D.; Aznauryan, M.; Gamrad, L.; Barcikowski, S.; Sanchez-Garcia, E.; Birkedal, V.; Gatsogiannis, C.; Ehrmann, M.; Saccà, B. Tailored protein encapsulation into a DNA host using geometrically organized supramolecular interactions. *Nat. Commun.* **2017**, *8*, 14472.
(8) Kwon, P. S.; Ren, S.; Kwon, S.-J.; Kizer, M. E.; Kuo, L.; Xie, M.; Zhu, D.; Zhou, F.; Zhang, F.; Kim, D.; Fraser, K.; Kramer, L. D.; Seeman, N. C.; Chao, J.; Wang, X. Designer DNA architecture offers precise and multivalent spatial pattern-recognition for viral sensing and inhibition. *Nat. Chem.* **2020**, *12*, 26−35.
(9) Sun, M.; Liu, S.; Wei, X.; Wan, S.; Huang, M.; Song, T.; Lu, Y.; Weng, X.; Lin, Z.; Chen, H.; Song, Y.; Yang, C. Aptamer blocking strategy inhibits SARS-CoV-2 virus infection. *Angew. Chem., Int. Ed.* **2021**, *60*, 10266−10272.
(10) Thiviyanathan, V.; Gorenstein, D. G. Aptamers and the next generation of diagnostic reagents. *Proteom. Clin. Appl.* **2012**, *6*, 563−573.
(11) Mammen, M.; Choi, S.-K.; Whitesides, G. M. Polyvalent interactions in biological systems: Implications for design and use of multivalent ligands and inhibitors. *Angew. Chem., Int. Ed.* **1998**, *37*, 2754−2794.
(12) Rangel, A. E.; Hariri, A. A.; Eisenstein, M.; Soh, H. T. Engineering Aptamer Switches for Multifunctional Stimulus-Responsive Nanosystems. *Adv. Mater.* **2020**, *32*, 2003704.
(13) Vazin, T.; Ashton, R. S.; Conway, A.; Schaffer, D. V. The effect of multivalent Sonic hedgehog on differentiation of human embryonic stem cells into dopaminergic and GABAergic neurons. *Biomaterials* **2014**, *35*, 941−948.
(14) Ehrlich, P. H. The effect of multivalency on the specificity of protein and cell interactions. *J. Theor. Biol.* **1979**, *81*, 123−127.
(15) Liu, F.; Walters, K. J. Multitasking with ubiquitin through multivalent interactions. *Trends Biochem. Sci.* **2010**, *35*, 352−360.
(16) Kiessling, L. L.; Gestwicki, J. E.; Strong, L. E. Synthetic multivalent ligands as probes of signal transduction. *Angew. Chem., Int. Ed.* **2006**, *45*, 2348−2368.
(17) Rao, J.; Lahiri, J.; Weis, R. M.; Whitesides, G. M. A trivalent system from vancomycin center dot D-Ala-D-Ala with higher affinity than avidin center dot biotin. *Science* **1998**, *280*, 708−711.
(18) Rao, J.; Lahiri, J.; Weis, R. M.; Whitesides, G. M. Design, synthesis, and characterization of a high-affinity trivalent system derived from vancomycin and L-Lys-D-Ala-D-Ala. *J. Am. Chem. Soc.* **2000**, *122*, 2698−2710.
(19) Varner, C. T.; Rosen, T.; Martin, J. T.; Kane, R. S. Recent advances in engineering polyvalent biological interactions. *Biomacromolecules* **2015**, *16*, 43−55.
(20) (a) Anslyn, E. V.; Dougherty, D. A. *Modern Physical Organic Chemistry*; University Science Books: Sausalito, CA, 2004. (b) Nangreave, J.; Yan, H.; Liu, Y. DNA Nanostructures as models for evaluating the role of enthalpy and entropy in polyvalent binding. *J. Am. Chem. Soc.* **2011**, *133*, 4490−4497.
(21) Aghebat Rafat, A.; Sagredo, S.; Thalhammer, M.; Simmel, F. C. Barcoded DNA origami structures for multiplexed optimization and enrichment of DNA-based protein-binding cavities. *Nat. Chem.* **2020**, *12*, 852−859.
(22) Rinker, S.; Ke, Y.; Liu, Y.; Yan, H.; Yan, R. Self-assembled DNA nanostructures for distance-dependent multivalent ligand-protein binding. *Nat. Nanotechnol.* **2008**, *3*, 418−422.
(23) Zhou, Y.; Qi, X.; Liu, Y.; Zhang, F.; Yan, H. DNA-nanoscaffold-assisted selection of femtomolar bivalent human α-thrombin aptamers with potent anticoagulant activity. *ChemBioChem* **2019**, *20*, 2494−2503.
(24) Krissanaprasit, A.; Key, C.; Fergione, M.; Froehlich, K.; Pontula, S.; Hart, M.; Carriel, P.; Kjems, J.; Sloth Andersen, E.; LaBean, T. H. Genetically encoded, functional single-strand RNA origami: anticoagulant. *Adv. Mater.* **2019**, *31*, No. e1808262.
(25) Rangnekar, A.; Zhang, A. M.; Li, S. S.; Bompiani, K. M.; Hansen, M. N.; Gothelf, K. V.; Sullenger, B. A.; LaBean, T. H. Increased anticoagulant activity of thrombin-binding DNA aptamers by nanoscale organization on DNA nanostructures. *Nanomedicine* **2012**, *8*, 673−681.
(26) Zhou, C.; Yang, Z.; Liu, D. Reversible regulation of protein binding affinity by a DNA machine. *J. Am. Chem. Soc.* **2012**, *134*, 1416−1418.
(27) Wang, J.; Wei, Y.; Hu, X.; Fang, Y.-Y.; Li, X.; Liu, J.; Wang, S.; Yuan, Q. Protein activity regulation: Inhibition by closed-loop aptamer-based structures and restoration by near-IR stimulation. *J. Am. Chem. Soc.* **2015**, *137*, 10576−10584.
(28) Kim, Y.; Cao, Z.; Tan, W. Molecular assembly for high-performance bivalent nucleic acid inhibitor. *Proc. Natl. Acad. Sci. U.S.A.* **2008**, *105*, 5664−5669.
(29) Müller, J.; Wulffen, B.; Pötzsch, B.; Mayer, G. Multidomain targeting generates a high-affinity thrombin-inhibiting bivalent aptamer. *ChemBioChem* **2007**, *8*, 2223−2226.
(30) Hasegawa, H.; Taira, K.-i.; Sode, K.; Ikebukuro, K. Improvement of aptamer affinity by dimerization. *Sensors* **2008**, *8*, 1090−1098.
(31) Ahmad, K. M.; Xiao, Y.; Soh, H. T. Selection is more intelligent than design: improving the affinity of a bivalent ligand through directed evolution. *Nucleic Acids Res.* **2012**, *40*, 11777−11783.
(32) Tasset, D. M.; Kubik, M. F.; Steiner, W. Oligonucleotide inhibitors of human thrombin that bind distinct epitopes. *J. Mol. Biol.* **1997**, *272*, 688−698.
(33) Russo Krauss, I.; Pica, A.; Merlino, A.; Mazzarella, L.; Sica, F. Duplex-quadruplex motifs in a peculiar structural organization cooperatively contribute to thrombin binding of a DNA aptamer. *Acta Crystallogr. Sect. D-Biol. Crystallogr.* **2013**, *69*, 2403−2411.
(34) Spiridonova, V. A.; Barinova, K. V.; Glinkina, K. A.; Melnichuk, A. V.; Gainutdynov, A. A.; Safenkova, I. V.; Dzantiev, B. B. A family of DNA aptamers with varied duplex region length that forms complexes with thrombin and prothrombin. *FEBS Lett.* **2015**, *589*, 2043−2049.
(35) Ikebukuro, K.; Okumura, Y.; Sumikura, K.; Karube, I. A novel method of screening thrombin-inhibiting DNA aptamers using an evolution-mimicking algorithm. *Nucleic Acids Res.* **2005**, *33*, e108.

https://doi.org/10.1021/jacs.1c12593
J. Am. Chem. Soc. 2022, 144, 4507−4514

(36) Russo Krauss, I.; Spiridonova, V.; Pica, A.; Napolitano, V.; Sica, F. Different duplex/quadruplex junctions determine the properties of anti-thrombin aptamers with mixed folding. *Nucleic Acids Res.* **2016**, *44*, 983−991.
(37) Bock, L. C.; Griffin, L. C.; Latham, J. A.; Vermaas, E. H.; Toole, J. J. Selection of single-stranded DNA molecules that bind and inhibit human thrombin. *Nature* **1992**, *355*, 564−566.
(38) Emsley, P.; Cowtan, K. Coot: model-building tools for molecular graphics. *Acta Crystallogr. Sect. D Biol. Crystallogr.* **2004**, *60*, 2126−2132.
(39) Dibrov, S. M.; McLean, J.; Parsons, J.; Hermann, T. Self-assembling RNA square. *Proc. Natl. Acad. Sci. U.S.A.* **2011**, *108*, 6405−6408.
(40) Zuo, H.; Wu, S.; Li, M.; Li, Y.; Jiang, W.; Mao, C. A case study of the likes and dislikes of DNA and RNA in self-assembly. *Angew. Chem., Intl. Ed.* **2015**, *54*, 15118−15121.
(41) Chi, Q.; Wang, G.; Jiang, J. The persistence length and length per base of single-stranded DNA obtained from fluorescence correlation spectroscopy measurements using mean field theory. *Phys. A: Stat. Mech. Appl.* **2013**, *392*, 1072−1079.
(42) Poppleton, E.; Romero, R.; Mallya, A.; Rovigatti, L.; Šulc, P. OxDNA.org: a public webserver for coarse-grained simulations of DNA and RNA nanostructures. *Nucleic Acids Res.* **2021**, *49*, W491−W498.
(43) Poppleton, E.; Bohlin, J.; Matthies, M.; Sharma, S.; Zhang, F. Design, optimization and analysis of large DNA and RNA nanostructures through interactive visualization, editing and molecular simulation. *Nucleic Acids Res.* **2020**, *48*, No. e72.
(44) Williams, S.; Lund, K.; Lin, C.; Wonka, P.; Lindsay, S.; Yan, H. Tiamat: A three-dimensional editing tool for complex DNA structures.In *DNA Computing. DNA 2008. Lecture Notes in Computer Science*; Goel, A., Simmel, F. C., Sosík, P. eds; Springer: Berlin, Heidelberg, Vol. *5347*, 2009.
(45) Sjekloća, L.; Ferré-D'Amaré, A. R. Binding between G quadruplexes at the homodimer interface of the Corn RNA aptamer strongly activates thioflavin T fluorescence. *Cell Chem. Biol.* **2019**, *26*, 1159−1168.

https://doi.org/10.1021/jacs.1c12593
J. Am. Chem. Soc. 2022, 144, 4507−4514